It is well known that the autonomic nervous system plays an important role on the arrhythmogenesis of Brugada syndrome. Previous studies showed that the withdrawal of sympathetic activity and the sudden rise in vagal activity was an important triggering factor of ventricular fibrillation.[13-15] Similarly, it has been presumed that parasympathetic tone increase during NMS events in patients with Brugada ECG. Recent basic study showed that *SCN5A*, a major responsible gene in Brugada patients, is expressed not only in the myocardial cells but also in intracardiac ganglia.[16] Makita *et al.* also demonstrated a novel nonsense mutation in *SCN5A* gene in a patient with Brugada syndrome who had been diagnosed as NMS.[17] These results suggested that the abnormal regulation or imbalance of autonomic nervous system may exist regardless of the presence or absence of cardiac events in patients with Brugada ECG.

ST-Segment Elevation in the Precordial Leads During the HUT Test in Patients with Brugada ECG

In Brugada syndrome, spontaneous augmentation of ST-segment elevation occurred along with an increase in vagal activity, especially just before and after the occurrence of ventricular fibrillation.[14] The ST-segment elevation is also known to be modulated by exercise,[18] pharmacological interventions that interact with automatic nervous activities,[19] or taking meals associated with glucose-induced insulin levels.[20] In this study, ST-segment augmentation in the right precordial leads was observed just before and after positive responses to the HUT test in two-thirds (69%) of the HUT-positive patients with Brugada ECG but only in 7% of the HUT-negative patients. In patients with Brugada ECG, the preceding increase of sympathetic nerve activity during the HUT test may cause augmentation of ICa-L, resulting in attenuation of ST-segment elevation.[19] Subsequent augmentation of parasympathetic nerve activity during the HUT test may decrease of ICa-L, and increase Ito, thus augmenting ST-segment amplitude.

Clinical Implication

The second consensus report suggested that symptomatic patients displaying type 1 Brugada ECG (either spontaneous or after class Ic drugs) who present with aborted sudden death should undergo ICD implantation.[3] ICD implantation is also recommended in patients with syncope, seizure, or nocturnal agonal respiration, after noncardiac causes of these symptoms have been carefully ruled out.[3] Needless to say, the ECG recording during syncope is the only convincing way to rule in or out VT during syncope, and only clinical judgment can be used to guide diagnostic and therapeutic decisions. However, in patients with Brugada syndrome, there is an abnormal regulatory imbalance of the autonomic nervous system that may be a common denominator to both syncope and ventricular fibrillation.

Limitations

The control subjects were significantly younger than patients with Brugada ECG or those with suspected NMS. However, it is reported that the positive rate of NTG-Tilt in the elderly was comparable to that seen in younger subjects.[21] Therefore, lower incidence of positive rate of the HUT test in the control subjects than that in the other 2 groups was not due to the relevant difference of age. The incidence of spontaneous type 1 ECG and the positive rate of the HUT test are smaller in Brugada patients with syncope episodes only than in those with documented VT or asymptomatic patients; however, statistical significance was not observed between the 3 groups.

Conclusions

Thirty-five percent of patients with Brugada ECG showed vasovagal responses during the HUT test. The HUT test was also positive in 41% among only Brugada patients with documented VT or no symptoms. During vasovagal response, ST-segment augmentation in the right precordial leads was observed in 69% of the HUT-positive Brugada patients, but no ventricular arrhythmias were induced. These data suggest that some Brugada patients have impaired balance of autonomic nervous system, which may relate to their syncopal episodes. Additional studies including a large number of subjects are needed to validate our findings and possibly evaluate the role of the HUT test in risk stratification of patients with Brugada ECG.

References

1. Brugada P, Brugada J: Right bundle branch block, persistent ST segment elevation and sudden cardiac death: A distinct clinical and electrocardiographic syndrome. A multicenter report. J Am Coll Cardiol 1992;20:1391-1396.
2. Wilde AA, Antzelevitch C, Borggrefe M, Brugada J, Brugada R, Brugada P, Corrado D, Hauer RN, Kass RS, Nademanee K, Priori SG, Towbin JA, Study Group on the Molecular Basis of Arrhythmias of the European Society of Cardiology: Proposed diagnostic criteria for the Brugada syndrome: Consensus report. Circulation 2002;106:2514-2519.
3. Antzelevitch C, Brugada P, Borggrefe M, Brugada J, Brugada R, Corrado D, Gussak I, LeMarec H, Nademanee K, Perez Riera AR, Shimizu W, Schulze-Bahr E, Tan H, Wilde A: Brugada syndrome: Report of the second consensus conference: Endorsed by the Heart Rhythm Society and the European Heart Rhythm Association. Circulation 2005;111:659-670.
4. Brignole M, Alboni P, Benditt D, Bergfeldt L, Blanc JJ, Bloch Thomsen PE, van Dijk JG, Fitzpatrick A, Hohnloser S, Janousek J, Kapoor W, Kenny RA, Kulakowski P, Moya A, Raviele A, Sutton R, Theodorakis G, Wieling W, Task Force on Syncope, European Society of Cardiology: Guidelines on management (diagnosis and treatment) of syncope. Eur Heart J 2001;22:1256-1306.
5. Nowak L, Nowak FG, Janko S, Dorwarth U, Hoffmann E, Botzenhardt F: Investigation of various types of neurocardiogenic response to head-up tilting by extended hemodynamic and neurohumoral monitoring. Pacing Clin Electrophysiol 2007;30:623-630.
6. Dalla PR, Kleinmann A, Zysk S, Bechtold S, Netz N: Head-up-tilt testing in children: New perspectives using beat-to-beat blood-pressure monitoring. Images Paediatr Cardiol 2005;22:1-7.
7. Boysen A, Lewin MA, Hecker W, Leichter HE, Uhlemann F: Autonomic function testing in children and adolescents with diabetes mellitus. Pediatr Diabetes 2007;8:261-264.
8. Yamasaki F, Sato T, Sugimoto K, Takata J, Chikamori T, Sasaki M, Doi Y: Effect of diltiazem on sympathetic hyperactivity in patients with vasospastic angina as assessed by spectral analysis of arterial pressure and heart rate variability. Am J Cardiol 1998;81:137-140.
9. Pagani M, Lombardi F, Guzzetti S, Rimoldi O, Furlan R, Pizzinelli P, Sandrone G, Malfatto G, Dell'Orto S, Piccaluga E: Power spectral analysis of heart rate and arterial pressure variabilities as a marker of sympatho-vagal interaction in man and conscious dog. Circ Res 1986;59:178-193.
10. Márquez MF, Rivera J, Hermosillo AG, Iturralde P, Colín L, Moragrega JL, Cárdenas M: Arrhythmic storm responsive to quinidine in a patient with Brugada syndrome and vasovagal syncope. Pacing Clin Electrophysiol 2005;28:870-873.
11. Patruno N, Pontillo D, Anastasi R, Sunseri L, Giamundo L, Ruggeri G: Brugada syndrome and neurally mediated susceptibility. Ital Heart J 2005;6:761-764.

12. Samniah N, Iskos D, Sakaguchi S, Lurie KG, Benditt DG: Syncope in pharmacologically unmasked Brugada syndrome: Indication for an implantable defibrillator or an unresolved dilemma? Europace 2001;3:159-163.
13. Wichter T, Matheja P, Eckardt L, Kies P, Schäfers K, Schulze-Bahr E, Haverkamp W, Borggrefe M, Schober O, Breithardt G, Schäfers M: Cardiac autonomic dysfunction in Brugada syndrome. Circulation 2002;105:702-706.
14. Kasanuki H, Ohnishi S, Ohtuka M, Matsuda N, Nirei T, Isogai R, Shoda M, Toyoshima Y, Hosoda S: Idiopathic ventricular fibrillation induced with vagal activity in patients without obvious heart disease. Circulation 1997;95:2277-2285.
15. Matsuo K, Kurita T, Inagaki M, Kakishita M, Aihara N, Shimizu W, Taguchi A, Suyama K, Kamakura S, Shimomura K: The circadian pattern of the development of ventricular fibrillation in patients with Brugada syndrome. Eur Heart J 1999;20:465-470.
16. Scornik FS, Desai M, Brugada R, Guerchicoff A, Pollevick GD, Antzelevitch C, Pérez GJ: Functional expression of "cardiac-type" Nav1.5 sodium channel in canine intracardiac ganglia. Heart Rhythm 2006;3:842-850.
17. Makita N, Sumitomo N, Watanabe I, Tsutsui H: Novel SCN5A mutation (Q55X) associated with age-dependent expression of Brugada syndrome presenting as neurally mediated syncope. Heart Rhythm 2007;4:516-519.
18. Grimster A, Segal OR, Behr ER. Type I Brugada electrocardiogram pattern during the recovery phase of exercise testing. Europace 2008;10:897-898.
19. Miyazaki T, Mitamura H, Miyoshi S, Soejima K, Aizawa Y, Ogawa S: Autonomic and antiarrhythmic drug modulation of ST segment elevation in patients with Brugada syndrome. J Am Coll Cardiol 1996;27:1061-1070.
20. Nishizaki M, Sakurada H, Mizusawa Y, Niki S, Hayashi T, Tanaka Y, Maeda S, Fujii H, Ashikaga T, Yamawake N, Isobe M, Hiraoka M. Influence of meals on variations of ST segment elevation in patients with Brugada syndrome. J Cardiovasc Electrophysiol 2008;19:62-68.
21. Tan MP, Parry SW: Vasovagal syncope in the older patient. J Am Coll Cardiol 2008;51:599-606.

ORIGINAL ARTICLE Arrhythmia/Electrophysiology *Circ J* 2009; **73:** 1028–1032

QRS Prolongation is Associated With High Defibrillation Thresholds During Cardioverter-Defibrillator Implantations in Patients With Hypertrophic Cardiomyopathy

Takayuki Nagai, MD; Takashi Kurita, MD; Kazuhiro Satomi, MD; Takashi Noda, MD; Hideo Okamura, MD; Wataru Shimizu, MD; Kazuhiro Suyama, MD; Naohiko Aihara, MD; Junjiro Kobayashi, MD*; Shiro Kamakura, MD

Background: Although high defibrillation threshold (DFT) is a major and unavoidable clinical problem after implantation of an implantable cardioverter defibrillator (ICD), little is known about the cause and management of a high DFT in patients with hypertrophic cardiomyopathy (HCM). The purpose of this study was to assess the predictors of a high DFT in patients with HCM.

Methods and Results: Twenty-three patients with non-dilated HCM who underwent ICD implantation were included. The DFT at the time of the device implantation was measured in all patients. The patients were divided into 2 groups, a high DFT group (DFT ≥15J, n=13) and a low DFT group (DFT <15J, n=10); and their baseline characteristics were compared. The QRS duration was longer in the high than in the low DFT group (128±31 vs 103±12 ms, respectively; P=0.02). QRS duration, left ventricular (LV) end-systolic diameter, and LV ejection fraction were significant predictors of DFT in univariate analysis. However, in multivariate analysis, the only factor significantly associated with DFT was QRS duration (P=0.002).

Conclusions: QRS duration is the most consistent predictor of a high DFT in HCM patients undergoing ICD implantation. (*Circ J* 2009; **73:** 1028–1032)

Key Words: Defibrillation threshold; Hypertrophic cardiomyopathy; Implantable cardioverter defibrillator; QRS prolongation

A subgroup of patients with hypertrophic cardiomyopathy (HCM) is at a high risk of having ventricular tachycardia and/or ventricular fibrillation. The implantable cardioverter-defibrillator (ICD) is widely recognized as the most effective and essential therapy for this patient population[1–3] It has been demonstrated that both appropriate and inappropriate ICD discharges are frequently observed in HCM patients[1–3] and this might impair quality-of-life as well as reduce battery longevity. Class III antiarrhythmic agents such as amiodarone have the potential for reducing ICD shocks[4] and might improve patients' prognosis. Furthermore, class I agents are also used in HCM patients to control atrial fibrillation or reduce the pressure gradient in the left ventricular (LV) outflow tract or midventricle when an obstruction is present[5–7] The combined use of antiarrhythmic agents and an ICD in patients with HCM, and the larger volume of myocardium (caused by hypertrophy of the left ventricle) might result in a high defibrillation threshold (DFT). However, the predictors of a high DFT in patients with HCM have not been fully characterized. Thus, the purpose of this retrospective study was to evaluate the factors causing a high DFT in patients with HCM and ventricular tachycardia/ventricular fibrillation.

(Received July 31, 2008; revised manuscript received January 7, 2009; accepted January 15, 2009; released online April 10, 2009)
*Division of Cardiology, Department of Internal Medicine, *Department of Cardiovascular Surgery, National Cardiovascular Center, Suita, Japan*
Mailing address: Takashi Kurita, MD, Division of Cardiology, Department of Internal Medicine, National Cardiovascular Center, 5-7-1 Fujishiro-dai, Suita 565-8565, Japan. E-mail: kuritat@hsp.ncvc.go.jp

Methods

Study Subjects

The study population consisted of 23 consecutive patients with an established diagnosis of HCM who underwent initial implantation of an ICD with a standard transvenous lead system at the National Cardiovascular Center from 1997 through to 2005. ICDs were implanted for secondary prevention in 20 of 23 patients, defined by clinical sustained ventricular tachyarrhythmia or resuscitation from sudden cardiac death. HCM was diagnosed on the basis of echocardiographic criteria defined as the presence of LV hypertrophy in the absence of other causes of hypertrophy. These patients also met the definition and classification proposed by the 1995 World Health Organization/International Society and Federation of Cardiology Task Force[8] All defibrillation leads were implanted by a left cephalic vein cutdown and positioned in the right ventricular apex. No patient had any prior pacemaker implantation, and 2 had permanent atrial fibrillation. Patients who were diagnosed with HCM who progressed to a dilated phase of HCM were excluded from the study.

ICD Implantation and DFT Testing

The following ICD models were implanted: 7220C (n=1), 7223Cx (n=6), 7227Cx (n=2), 7229Cx (n=5), 7271Cx (n=1), and 7273Cx (n=5), manufactured by Medtronic, Inc (Minneapolis, MN, USA); and the 1861 (n=3) manufac-

Table 1. Patient Characteristics

	Defibrillation threshold		P value
	<15J (n=10)	≥15J (n=13)	
Gender (M/F)	7/3	9/4	NS
Age, years	52±18	54±16	NS
Height, cm	163±8	162±8	NS
Body weight, kg	55±9	59±7	NS
QRS duration, ms	103±12	128±31	0.02
LV ejection fraction, %	68±16	58±10	0.09
Defibrillation threshold, J	10±0.4	18±5	0.0001
Antiarrhythmic agents, n (%)	3 (30)	6 (46)	NS
Amiodarone, n (%)	2 (20)	4 (31)	NS
Disopyramide, n (%)	1 (10)	1 (8)	NS
Mexiletine, n (%)	0 (0)	2 (15)	NS
Single coil lead system, n (%)	9 (90)	8 (62)	NS

Data are mean±SD.
NS, not significant; LV, left ventricular.

Table 2. Echocardiographic Measurements

	Defibrillation threshold		P value
	<15J (n=10)	≥15J (n=13)	
LV end-diastolic diameter, mm	39±6	42±6	NS
LV end-systolic diameter, mm	22±6	26±5	0.048
Interventricular septal thickness, mm	17±5	18±6	NS
LV posterior wall thickness, mm	13±3	14±8	NS
LV mass, g	286±124	369±211	NS
LV mass index, g/m^2	178±64	227±126	NS

Data are mean±SD.
Abbreviations see in Table 1.

tured by Guidant Corp (St. Paul, MN, USA). All ICD systems used biphasic waveforms. A single-coil transvenous lead system was utilized in 17 patients and a dual-coil system was used in 6 patients. All implant procedures were performed under general anesthesia using propofol in the operating room. At the end of the ICD implantation after ventricular fibrillation was induced using a T-wave shock or 50-Hz burst pacing, DFT was measured using a step-down method from an initial delivered energy of 15J with decrements of 5J[9,10] If the initial 15J shock failed, the energy was increased in 5J steps until defibrillation was successful. A 5-min interval was allowed between inductions and defibrillations of ventricular fibrillation. The DFT was defined as the lowest delivered energy shock that resulted in a successful defibrillation. According to the mean value of DFT (14±5J), the patients were classified into 10 patients with a low DFT (<15J) and 13 patients with a high DFT (≥15J).

Variables Assessed

The following variables were used for analysis: sex, age, height, body weight, QRS duration, LV ejection fraction quantified by radionuclide ventriculography or LV cineangiography, the use of amiodarone or class I antiarrhythmic drugs, utilization of a single-coil transvenous lead system, echocardiographic parameters including the LV end-diastolic and end-systolic diameters, interventricular septal thickness, LV posterior wall thickness, LV mass calculated from echocardiographic data by standard formulas[11,12] and LV mass index (dividing the LV mass by the body surface area). The QRS duration was defined as the maximal QRS length in any lead measured manually from the first to the last sharp deflection crossing the isoelectric line using standard resting 12-lead ECG (sweep speed, 25 mm/s and 1 mV/cm standardization). The average values of QRS duration that were obtained from 2 independent investigators blinded to each other's results were used (interobserver correlation for QRS duration was 0.941).

Statistical Analysis

The results are presented as percentages or the mean±SD, as appropriate. Several parameters in the 2 groups were compared with an unpaired Student's t-test. Categorical variables were compared using a Fisher's exact test. Linear regression analysis was used to determine the relationship between DFT and QRS duration. The variables with a P value <0.10 were entered into a multiple linear regression analysis to identify the independent predictors of DFT. The level of statistical significance was set at a P value <0.05.

Results

Twenty-three patients (16 men; mean age 53±17 years, range 16–77 years) were included in the analysis. None of the patients had any extreme hypertrophy (≥30 mm), and 4 patients were found to have significant LV outflow obstruction (≥30 mmHg) at rest by continuous Doppler echocardiography. The mean LV ejection fraction was 62±13%. Indications for an ICD implantation were primary prevention in 3 patients, ventricular tachycardia in 4 patients and aborted sudden cardiac death in 16 patients. At the time of device implantation, 6 patients were being treated with amiodarone (200 mg/day), 2 with sotalol and 4 with class I antiarrhythmic agents (disopyramide and mexiletine). No patient showed evidence of abnormalities in serum electrolyte concentrations and/or in acid–base equilibrium at the device implantation stage.

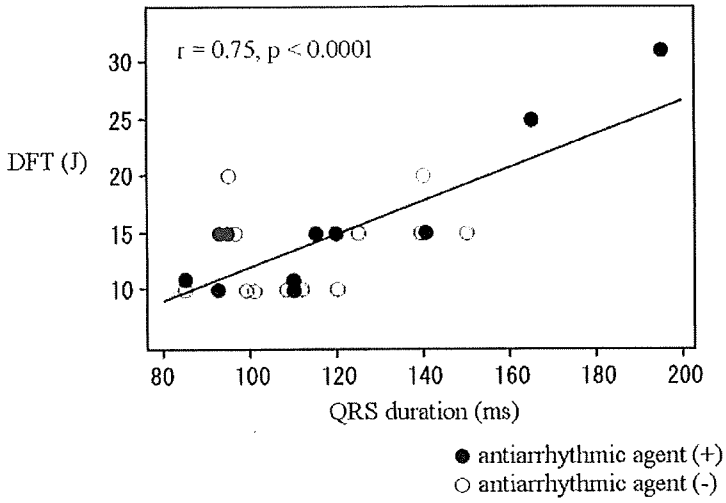

Figure. Relationship between QRS duration and DFT. The QRS duration demonstrated a modest positive correlation with the DFT at the time of the device implantation. DFT, defibrillation threshold.

The ICDs were implanted without any complications, and the induction and termination of the ventricular fibrillation were successful in all patients. The DFT (energy delivered) ranged from 10J to 31J (10 patients, 10–14J; 9 patients, 15–19J; 2 patients, 20–24J; 2 patients, 25–31J). The DFTs in patients treated with amiodarone (6 patients), combined amiodarone and a class I antiarrhythmic agent (mexiletine) (1 patient), class I antiarrhythmic agents (3 patients), and sotalol (2 patients) were 16±9J, 15J, 17±7J, and 13±3J, respectively. An unacceptably high DFT (≥25J) was obtained in 2 patients who were receiving amiodarone (1 patient, 200 mg/day) or mexiletine (1 patient, 450 mg/day) at the time of the implantation (these 2 patients were included in the high DFT group). However, the DFT in these 2 patients decreased to a level with a 10J safety margin between the maximum shock energy of the ICD and the DFT after cessation of amiodarone (21J) or mexiletine (20J). Therefore, none of the patients required any additional use of a subcutaneous array or patch.

The baseline characteristics and echocardiographic measurements for the 2 groups are listed in **Tables 1** and **2**, respectively. The QRS duration was significantly longer in patients with a high than with a low DFT (128±31 vs 103± 12 ms, respectively; P=0.02). There was a trend toward a lower LV ejection fraction in the patients with a high DFT (P=0.09). The use of amiodarone and/or class I antiarrhythmic drugs did not differ between the 2 groups. As shown in **Table 2**, the LV end-systolic diameter was significantly smaller in those patients with a low than with a high DFT (22±6 vs 26±5 mm, respectively; P=0.048). The LV mass and mass index exhibited no statistically significant difference between the 2 groups.

The QRS duration demonstrated a modest positive correlation with the DFT at the time of device implantation (r= 0.75, P<0.0001) for the group as a whole (**Figure**). A multivariate analysis was performed on the 3 variables that had a P value <0.10 in the univariate analysis: QRS duration, LV end-systolic diameter, and LV ejection fraction. This analysis showed that QRS duration was the only independent predictor of DFT (P=0.002).

Discussion

In this study, we identified QRS duration as the only variable that was associated with a high DFT at the time of ICD implantation in patients with HCM. To the best of our knowledge, this is the first report to investigate the association between QRS duration and DFT in patients with HCM. Because of the pro-arrhythmic and/or negative inotropic effects of class I antiarrhythmic agents, the use of these drugs in patients with depressed LV function is contraindicated. Furthermore, class Ia antiarrhythmic drugs such as disopyramide or cibenzoline might lead to a rise in DFT by producing a wider zone between the resting membrane potential and threshold potential![3] However, class Ia antiarrhythmic agents have been regarded as part of the standardized therapy, not only for reducing LV pressure gradients[5–7] in patients with obstructive HCM, but also for improving LV diastolic dysfunction even in patients with non-obstructive HCM![14,15] Therefore, it is even more important to predict an increase in DFT before ICD implantation in patients with HCM. Previous studies have described several clinical factors that are associated with a high DFT, such as LV dilatation![16] body size![16] decreased LV ejection fraction![17] administration of antiarrhythmic drugs (class I; flecainide![18] mexiletine[19,20] etc, class III; amiodarone[21–23]), myocardial ischemia![24–27] the ventricular fibrillation duration![28,29] and LV mass![23,30,31] Among these factors possibly associated with high DFTs, only the LV ejection fraction was found to be a univariate predictor of a high DFT in the present study. This might be because HCM exhibits a unique structural and electrophysiologic substrate in the myocardium. Almquist et al reported that extreme LV hypertrophy (wall thickness >45 mm) and the administration of amiodarone were related to a high DFT in patients with HCM![32] The LV mass index was slightly larger in the high than in the low DFT group in spite of the absence of any extreme LV hypertrophy in our series. Although this result was not statistically significant because of the small sample size, this suggests that a larger LV mass might increase the DFT.

QRS Duration and DFT

Although 2 published studies have shown an association between QRS duration and DFT, QRS duration was not an independent predictor of DFT in multivariate analysis![16,30] However, those study populations included mainly ischemic heart disease patients. This is the first study to investigate the association between QRS duration and DFT in patients

with HCM. Dhingra et al showed that QRS duration was positively related to LV mass and dimensions in individuals free of heart failure and myocardial infarction[33] However, there was no significant association between QRS duration and LV mass in our subjects. Asymmetric LV hypertrophy, which is frequently observed in HCM, might make it difficult to precisely evaluate LV mass in the clinical setting. This might be a possible explanation for our observed data.

Study Limitations

The results presented here must be viewed as preliminary as they are based on experience in a single center and in a small number of patients. Furthermore, this study was conducted retrospectively. In addition, we did not have any follow-up data on DFT after device implantation. All patients underwent the implantations under general anesthesia using propofol, as described above, which might have elevated the DFT[34] Thus, it is possible that the DFT in the operating room differed from that in the clinical setting. A further major limitation is the absence of a uniform strategy for the selection of lead systems and antiarrhythmic agents that could affect the DFT. Finally, 2 patients in this study who had unacceptably high DFTs obtained a 10-J safety margin after cessation of antiarrhythmic agents. Moreover, not all patients taking antiarrhythmic agents at the ICD implantation had their DFTs measured after discontinuation of antiarrhythmic agents. We report here that the QRS prolongation was associated with a high DFT at the time of ICD implantation in patients with HCM, leaving doubt as to how much the antiarrhythmic agents would affect high DFT and QRS prolongation. Additional studies in a larger patient population are needed to determine the impact of QRS duration on DFT, as well as the influence of antiarrhythmic agents on DFT, and the long-term consequences of an elevated DFT in HCM patients.

Clinical Implications

In patients with HCM, the presence of a QRS prolongation on the 12-lead ECG should raise concern about a high DFT at the time of ICD implantation, and those patients should be started at a higher energy level for DFT measurements using a high-output device to obtain an adequate safety margin for defibrillation. In the patients who have already been implanted with an ICD, antiarrhythmic agents, which might cause a high DFT, should be prescribed very carefully. Moreover, when QRS prolongation is present before drug administration, DFT testing is warranted after the initiation of drug therapy.

Conclusion

The present report revealed an association between the QRS duration and DFT at the time of ICD implantation in patients with HCM. This might provide an important insight into the link between simple 12-lead ECG markers and the energy requirements for successful defibrillation in patients with HCM.

References

1. Maron BJ, Shen WK, Link MS, Epstein AE, Almquist AK, Daubert JP, et al. Efficacy of implantable cardioverter-defibrillators for the prevention of sudden death in patients with hypertrophic cardiomyopathy. *N Engl J Med* 2000; **342:** 365–373.
2. Maron BJ, Estes NA 3rd, Maron MS, Almquist AK, Link MS, Udelson JE. Primary prevention of sudden death as a novel treatment strategy in hypertrophic cardiomyopathy. *Circulation* 2003; **107:** 2872–2875.
3. Begley DA, Mohiddin SA, Tripodi D, Winkler JB, Fananapazir L. Efficacy of implantable cardioverter defibrillator therapy for primary and secondary prevention of sudden cardiac death in hypertrophic cardiomyopathy. *Pacing Clin Electrophysiol* 2003; **26:** 1887–1896.
4. Lee CH, Nam GB, Park HG, Kim HY, Park KM, Kim J, et al. Effects of antiarrhythmic drugs on inappropriate shocks in patients with implantable cardioverter defibrillators. *Circ J* 2008; **72:** 102–105.
5. Sherrid MV, Barac I, McKenna WJ, Elliott PM, Dickie S, Chojnowska L, et al. Multicenter study of the efficacy and safety of disopyramide in obstructive hypertrophic cardiomyopathy. *J Am Coll Cardiol* 2005; **45:** 1251–1258.
6. Hamada M, Shigematsu Y, Ikeda S, Hara Y, Okayama H, Kodama K, et al. Class Ia antiarrhythmic drug cibenzoline: A new approach to the medical treatment of hypertrophic obstructive cardiomyopathy. *Circulation* 1997; **96:** 1520–1524.
7. Hamada M, Shigematsu Y, Inaba S, Aono J, Ikeda S, Watanabe K, et al. Antiarrhythmic drug cibenzoline attenuates left ventricular pressure gradient and improves transmitral Doppler flow pattern in patients with hypertrophic obstructive cardiomyopathy caused by midventricular obstruction. *Circ J* 2005; **69:** 940–945.
8. Richardson P, McKenna W, Bristow M, Maisch B, Mautner B, O'Connell J, et al. Report of the 1995 World Health Organization/International Society and Federation of Cardiology Task Force on the Definition and Classification of cardiomyopathies. *Circulation* 1996; **93:** 841–842.
9. Neuzner J, Liebrich A, Jung J, Himmrich E, Pitschner HF, Winter J, et al. Safety and efficacy of implantable defibrillator therapy with programmed shock energy at twice the augmented step-down defibrillation threshold: Results of the prospective, randomized, multicenter Low-Energy Endotak Trial. *Am J Cardiol* 1999; **83:** 34D–39D.
10. Rashba EJ, Olsovsky MR, Shorofsky SR, Kirk MM, Peters RW, Gold MR. Temporal decline in defibrillation thresholds with an active pectoral lead system. *J Am Coll Cardiol* 2001; **38:** 1150–1155.
11. Sahn DJ, DeMaria A, Kisslo J, Weyman A (the Committee on M-Mode Standardization of the American Society for Echocardiography). Recommendations regarding quantitation in M-mode echocardiography: Results of a survey of echocardiographic measurements. *Circulation* 1978; **58:** 1072–1083.
12. Devereux RB, Reichek N. Echocardiographic determination of left ventricular mass in man. Anatomic validation of the method. *Circulation* 1977; **55:** 613–618.
13. Babbs CF. Alteration of defibrillation threshold by antiarrhythmic drugs: A theoretical framework. *Crit Care Med* 1981; **9:** 362–363.
14. Hamada M, Shigematsu Y, Hara Y, Suzuki M, Ohtsuka T, Hiasa G, et al. Antiarrhythmic drug, cibenzoline, can directly improve the left ventricular diastolic function in patients with hypertrophic cardiomyopathy. *Jpn Circ J* 2001; **65:** 531–538.
15. Hamada M, Aono J, Ikeda S, Watanabe K, Inaba S, Suzuki J, et al. Effect of intravenous administration of cibenzoline on left ventricular diastolic pressures in patients with hypertrophic cardiomyopathy: Its relationship to transmitral Doppler flow profiles. *Circ J* 2007; **10:** 1540–1544.
16. Gold MR, Khalighi K, Kavesh NG, Daly B, Peters RW, Shorofsky SR. Clinical predictors of transvenous biphasic defibrillation thresholds. *Am J Cardiol* 1997; **79:** 1623–1627.
17. Pinski SL, Vanerio G, Castle LW, Morant VA, Simmons TW, Trohman RG, et al. Patients with a high defibrillation threshold: Clinical characteristics, management, and outcome. *Am Heart J* 1991; **122:** 89–95.
18. Reiffel JA, Coromilas J, Zimmerman JM, Spotnitz HM. Drug-device interactions: Clinical considerations. *Pacing Clin Electrophysiol* 1985; **8:** 369–373.
19. Yoon MS, Han J. Electrophysiologic effects of mexiletine on normal and ischemic ventricles. *J Electrocardiol* 1982; **15:** 109–113.
20. Marinchak RA, Friehling TD, Kline RA, Stohler J, Kowey PR. Effect of antiarrhythmic drugs on defibrillation threshold: Case report of an adverse effect of mexiletine and review of the literature. *Pacing Clin Electrophysiol* 1988; **11:** 7–12.
21. Khalighi K, Daly B, Leino EV, Shorofsky SR, Kavesh NG, Peters RW, et al. Clinical predictors of transvenous defibrillation energy requirements. *Am J Cardiol* 1997; **79:** 150–153.
22. Pelosi F Jr, Oral H, Kim MH, Sticherling C, Horwood L, Knight BP, et al. Effect of chronic amiodarone therapy on defibrillation energy requirements in humans. *J Cardiovasc Electrophysiol* 2000; **11:** 741–743.
23. Kopp DE, Blakeman BP, Kall JG, Olshansky B, Kinder CA, Wilber DJ. Predictors of defibrillation energy requirements with nonepicardial lead systems. *Pacing Clin Electrophysiol* 1995; **18:** 253–260.

24. Anastasiou-Nana MI, Tsagalou EP, Charitos C, Siafakas KX, Drakos S, Terrovitis JV, et al. Effects of transient myocardial ischemia on the ventricular defibrillation threshold. *Pacing Clin Electrophysiol* 2005; **28:** 97–101.
25. Babbs CF, Paris RL, Tacker WA Jr, Bourland JD. Effects of myocardial infarction on catheter defibrillation threshold. *Med Instrum* 1983; **17:** 18–20.
26. Qin H, Walcott GP, Killingsworth CR, Rollins DL, Smith WM, Ideker RE. Impact of myocardial ischemia and reperfusion on ventricular defibrillation patterns, energy requirements, and detection of recovery. *Circulation* 2002; **105:** 2537–2542.
27. Walcott GP, Killingsworth CR, Smith WM, Ideker RE. Biphasic waveform external defibrillation thresholds for spontaneous ventricular fibrillation secondary to acute ischemia. *J Am Coll Cardiol* 2002; **39:** 359–365.
28. Strobel JS, Kenknight BH, Rollins DL, Smith WM, Ideker RE. The effects of ventricular fibrillation duration and site of initiation on the defibrillation threshold during early ventricular fibrillation. *J Am Coll Cardiol* 1998; **32:** 521–527.
29. Windecker S, Ideker RE, Plumb VJ, Kay GN, Walcott GP, Epstein AE. The influence of ventricular fibrillation duration on defibrillation efficacy using biphasic waveforms in humans. *J Am Coll Cardiol* 1999; **33:** 33–38.
30. Hodgson DM, Olsovsky MR, Shorofsky SR, Daly B, Gold MR. Clinical predictors of defibrillation thresholds with an active pectoral pulse generator lead system. *Pacing Clin Electrophysiol* 2002; **25:** 408–413.
31. Chapman PD, Sagar KB, Wetherbee JN, Troup PJ. Relationship of left ventricular mass to defibrillation threshold for the implantable defibrillator: A combined clinical and animal study. *Am Heart J* 1987; **114:** 274–278.
32. Almquist AK, Montgomery JV, Haas TS, Maron BJ. Cardioverter-defibrillator implantation in high-risk patients with hypertrophic cardiomyopathy. *Heart Rhythm* 2005; **2:** 814–819.
33. Dhingra R, Ho Nam B, Benjamin EJ, Wang TJ, Larson MG, D'Agostino RB Sr, et al. Cross-sectional relations of electrocardiographic QRS duration to left ventricular dimensions: The Framingham Heart Study. *J Am Coll Cardiol* 2005; **45:** 685–689.
34. Cohen TJ, Chengot T, Quan C, Peller AP. Elevation of defibrillation thresholds with propofol during implantable cardioverter-defibrillator testing. *J Invasive Cardiol* 2000; **12:** 121–123.

Repolarization Spatial-Time Current Abnormalities in Patients with Coronary Heart Disease

KUNIOMI OGATA,* AKIHIKO KANDORI,* YASUSHI WATANABE,† AKIHIRO SUZUKI,† KIMIO TANAKA,† YUJI OKA,† HIROSHI TAKAKI,‡ HIDEAKI KANZAKI,‡ SATOSHI NAKATANI,‡ KUNIO MIYATAKE,‡ SHIGEYUKI WATANABE,§ IWAO YAMAGUCHI,§ TSUYOSHI MIYASHITA,* and SHIRO KAMAKURA‡

From the *Advanced Research Laboratory, Hitachi Ltd., Higashi-Koigakubo, Kokubunji, Tokyo, Japan; †Hitachi General Hospital, Ibaraki, Japan; ‡National Cardiovascular Center, Osaka, Japan; and §Institute of Clinical Medicine, University of Tsukuba, Ibaraki, Japan

Background: *Magnetocardiography (MCG) is a new technique for visualizing a current distribution in the myocardium. In recent years, current distribution parameters (CDPs) have been developed based on the distribution. The CDPs reflect spatial-time current abnormalities in patients with coronary heart disease (CHD). However, the criteria and scoring method of the abnormalities using CDPs are still controversial.*

Method: *We measured MCG signals for 101 normal controls and 56 CHD patients (single-, double-, and triple-vessel diseases) using a MCG system. The CDPs (maximum current vector [MCV], total current vector [TCV], current integral map, and current rotation) during ventricular repolarization were analyzed. To evaluate the CDPs that are effective in distinguishing between normal controls and CHD patients, the areas under the receiver operating characteristic curve (A_z) are calculated. Furthermore, the total scores ("0" to "4") of four CDPs with high A_z values are also calculated.*

Results: *MCV and TCV angles at the T-wave peak had the highest A_z value. Furthermore, TCV angular differences between the ST-T segment also had high A_z values. Using the four CDPs, the averaged total score for patients with triple-vessel disease was the highest ("2.67") compared to the other groups (normal controls: 0.53). Furthermore, based on the assumption that subjects with a total score over "1" were suspected of having CHD, sensitivity and specificity were 85.7% and 74.3%, respectively.*

Conclusion: *We concluded that the score and criteria using MCV and TCV during repolarization in CHD patients can reflect lesion areas and time changes of electrical activation dispersion due to ischemia. (PACE 2009; 32:516–524)*

magneticardiogram, coronary heart disease, cardiac electrical current

Introduction

The number of people throughout the world who die each year from coronary heart disease (CHD) is about 7 million and counting.[1] In Japan, more than 70,000 people have died of CHD, and this number has remained steady for the last decade.[2] Under the circumstances, several types of medical equipment that allow early diagnosis of CHD have been developed.[3–18]

The exercise-induced electrocardiogram (ECG)[3–5] with treadmill and ergometer exercise test helps to diagnose and assess the severity of CHD. This device can detect abnormal electrical potential changes in an exercise examination. Therefore, exercise-induced ECG is prevalent in an initial evaluation when CHD is suspected. However, some problems with this method include the burden on patients and the long time required for measurement.

The magnetocardiogram (MCG) is a new medical device that measures the weak magnetic field generated by the ionic current in the human heart.[6–11] It is a noninvasive technique that involves no contact with the human body. The MCG remains largely unaffected by other organs because permittivity of the human body is relatively constant. Therefore, the MCG is expected to be a useful system to detect the imperceptible changes in cardiac electrical activation that are caused by various heart diseases.

Some clinical research has been done based on magnetic field parameters (MFPs), which are calculated from MCG signals.[12,13] These MFPs are obtained from coordinates and amplitudes of maximum and minimum magnetic fields during the ventricular repolarization phase. Park et al. examined four MFPs during the ST to T-wave peak for 185 patients with ischemic syndrome.[12] Tolstrup et al. examined seven MFPs during the ST-T segment for 125 patients with chest pain.[13] These examinations showed that an MCG test using MFPs had high sensitivity and specificity for detection

Address for reprints: Kuniomi Ogata, Advanced Research Laboratory, Hitachi Ltd., 1-280 Higashi-Koigakubo, Kokubunji, Tokyo 185-8601, Japan. Fax: 81-42-327-7783; e-mail: kuniomi.ogata.fb@hitachi.com

Received August 20, 2007; revised March 13, 2008; accepted December 15, 2008.

of CHD. However, it is difficult to understand from MFPs how electrical current abnormalities (such as abnormal current amplitude, direction, and site) occurred in the myocardium.

However, MCG signals are converted into a cardiac electrical image. This image is generally obtained from a two-dimensional (2D) current-arrow map (CAM).[6,14] The CAM gives us a pseudo-2D electrical current distribution consisting of 2D arrows and contours representing the magnitude of arrows. The current distribution parameters (CDPs), which are calculated from the CAM, reflect spatial and time current abnormalities in patients with CHD and other heart diseases.[15–23] However, the criteria and scoring method of the abnormalities using CDPs are still controversial.

Method

Subjects

Table I contains the details of the study population, which consisted of 56 patients (46 males and 10 females) with CHD and 101 normal controls (70 males and 31 females). All of the patients were confirmed to have coronary artery lesions by coronary angiography (CAG). We defined the coronary heart lesions as a vessel diameter >75%. Of the patients, 25 had single-vessel disease (SVD) (right coronary artery disease in six, left anterior descending artery disease in 16, and left circumflex artery disease in three), 13 had double-vessel disease (DVD), and 18 had triple-vessel disease (TVD). Patients who had undergone cardiovascular therapy (coronary artery bypass grafting [CABG], or percutaneous coronary intervention [PCI]) were not included in this study. The normal controls consisted of healthy volunteers with no history of cardiovascular disease and who had a normal ECG at rest (see previous paper[19]). Informed consent was obtained from all subjects.

The members of the control group were selected on the basis of only the ECG results. Therefore, cardiac hypertrophy, dilation, and high blood pressure (HBP), which are measured with other heart functional tests, cannot be excluded in this study. Despite that some cardiac diseases were not completely excluded, we defined a normal control group from the ECG results because an electrophysiological test is used as a first step to diagnose cardiac disease. The CHD group was composed of persons who had coronary artery lesions confirmed by CAG.

Table I.

Clinical Characteristics of Subjects

	N (n = 101)	CHD (n = 56)
Age (years)	63 + 3	65 + 6
Gender		
Female/Male	31/70	10/46
BMI	23.7	24
HR (bpm)	63	63
Coronary status		
1-vessel		25
LAD		16
LCX		3
RCA		6
2-vessel		13
3-vessel		18

N = normal controls; CHD = patients with coronary heart disease (stenosis > 75%); BMI = body mass index; HR = heart rate; LAD = left anterior descending coronary artery; LCX = left circumflex coronary artery; RCA = right coronary artery.

MCG System and Data Acquisition

We used a Low-Tc superconducting quantum interference device (SQUID) system with 64 coaxial gradiometers (50-mm baseline and 18-mm diameter) to measure the axial component of the magnetic field (Hitachi High-Technologies Corporation, Tokyo, Japan). The gradiometers were in an 8 × 8 matrix with a pitch of 25 mm, and the measurement area was 175 × 175 mm. Figure 1 illustrates the configuration for the MCG measurement. To adjust the position of the measurement areas for each subject, one gradiometer (position 51) was placed above the position of the xiphoid process. The measured MCG signals at this position

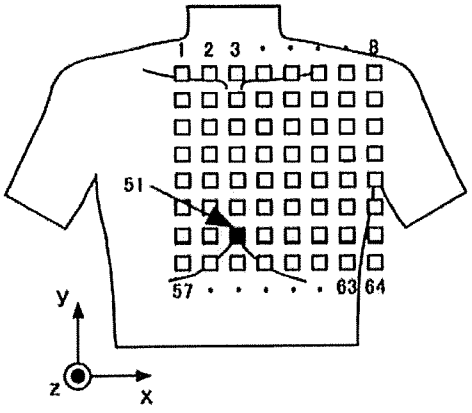

Figure 1. *Configuration for measurement of magnetocardiography (MCG) system (Hitachi High-Technologies Corporation). The 64 SQUID sensors are laid out in an 8 × 8 matrix; the sensor pitch is 25 mm. Channel no. 51 (black square) is placed above the position of the xiphoid process. The MCG system measures the normal component (z-component) of the magnetic field generated by the current in the myocardium.*

were acquired at a sampling rate of 1 kHz and passed through a bandpass (0.1 to 100 Hz) and power line noise filters. The maximum measurement period was 120 seconds, and the MCG signals for all pulses over this period were averaged. A lead II ECG was simultaneously measured as reference signals for MCG averaging.

Spatial and Time Identification of Current Distribution Using MCG

The amplitude and direction of cardiac electrical current vary with the electrical potential difference between normal and ischemic myocardium. To detect these current changes in the myocardium, we calculated CDPs based on maximum current vector (MCV), total current vector (TCV), current integral map (CIM), and current rotation (CR). With the MCV, it is possible to detect local changes in amplitude and direction of the cardiac current.[19] TCV reflects the averaged change in the primary current of the whole heart.[15,16,19] CIM represents the amount of cardiac current during the ventricular depolarization and repolarization phase.[17–19] Furthermore, with the CR, changes in the current distribution pattern can be detected.[21]

Maximum Current Vector

Averaged MCG signals are converted to a CAM. CAM is the method for reconstructing 2D pseudocardiac electrical current vectors at the same number of measurement points. Pseudo current vectors ($I_n = (I_{x,n}, I_{y,n})$) are calculated by taking the derivatives of the normal component ($B_{z,n}$) of the MCG signals at n^{th} sensor as

$$I_{x,n} = dB_{z,n}/dy \qquad (1)$$

and

$$I_{y,n} = -dB_{z,n}/dx. \qquad (2)$$

CAM can also be calculated by using the tangential components ($B_{y,z}$ and $B_{x,z}$) of the magnetic field instead of $dB_{z,n}/dy$ and $dB_{z,n}/x$ in equations (1) and (2). CAM gives us a spatial electrical activity consisting of 2D arrows ($I_{x,n}$ and $I_{y,n}$) and contours representing the magnitude of the arrows ($I_n = (I_x^2 + I_y^2)^{1/2}$).[14]

To evaluate the spatial current distribution and time variance of current distribution, we calculated the "amplitude ratio (I_{MCV})," "angle (θ_{MCV})," and "angle of difference current vector (φ_{MCV})" of a current arrow with MCV at four time instants (T_1, T_2, T_p, and T_e). The MCV ($I_{max} = (I_{x,max}, I_{y,max})$) indicates a vector with a maximal magnitude of arrows (I_n) at each time instant. Figure 2 schematically shows four time instants (T_1, T_2, T_p, and T_e). Here, T_1 ($T_1 = QRS_{on} + 0.18/\sqrt{(RR)}$) and T_2 ($T_2 = QRS_{on} + 0.20/\sqrt{(RR)}$) are time instants during the ST-T segment. QRS_{on} is the time instant at the beginning of the QRS complex, and RR indicates an averaged R-R interval. The term T_p is the T-wave peak time, and T_e ($T_e = T_p + (T_p - T_2)/2$) indicates time instants during the T-wave peak and the ending of the T wave.

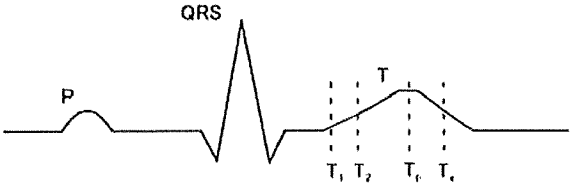

Figure 2. *Schematic representation of four time instants (T_1, T_2, T_p, and T_e) during ventricular repolarization.*

Using CAM at the four time instants, MCV parameters (I_{MCV}, θ_{MCV}, and φ_{MCV}) are calculated from the following equations

(1) I_{MCV}: amplitude ratio

$$\begin{aligned} I_{MCV}(T_2, T_1) &= (I_{max}(T_2) - I_{max}(T_1))/I_{max}(T_1) \\ I_{MCV}(T_p, T_2) &= (I_{max}(T_p) - I_{max}(T_2))/I_{max}(T_2), \\ I_{MCV}(T_p, T_e) &= (I_{max}(T_p) - I_{max}(T_e))/I_{max}(T_e) \end{aligned} \qquad (3)$$

(2) θ_{MCV}: angle

$$\begin{aligned} \theta_{MCV}(T_1) &= \tan^{-1}(I_{y,max}(T_1)/I_{x,max}(T_1)) \\ \theta_{MCV}(T_2) &= \tan^{-1}(I_{y,max}(T_2)/I_{x,max}(T_2)) \\ \theta_{MCV}(T_p) &= \tan^{-1}(I_{y,max}(T_{max})/I_{x,max}(T_p)) \\ \theta_{MCV}(T_e) &= \tan^{-1}(I_{y,max}(T_e)/I_{x,max}(T_e)) \end{aligned}, \qquad (4)$$

(3) φ_{MCV}: angle of difference current vector

$$\begin{aligned} \varphi_{MCV}(T_2, T_1) &= \tan^{-1}((I_{y,max}(T_2) - I_{y,max}(T_1)) \\ &\quad /(I_{x,max}(T_2) - I_{x,max}(T_1)) \\ \varphi_{MCV}(T_p, T_2) &= \tan^{-1}((I_{y,max}(T_p) - I_{y,max}(T_2)) \\ &\quad /(I_{x,max}(T_p) - I_{x,max}(T_2)) \\ \varphi_{MCV}(T_p, T_e) &= \tan^{-1}((I_{y,max}(T_p) - I_{y,max}(T_e)) \\ &\quad /(I_{x,max}(T_p) - I_{x,max}(T_2)) \end{aligned}, \qquad (5)$$

where the angles (θ_{MCV} and φ_{MCV}) are defined as in Figure 3A and B. Amplitude ratio (I_{MCV}) and angle of difference current vector (φ_{MCV}) were calculated from nearby time points (T_2 and T_1, T_p and T_2, T_p and T_e). Current amplitude and current angle during the ventricular repolarization phase slowly and continuously change for healthy subjects.[24] Therefore, we consider that such changes at nearby time points are proper parameters for detecting abnormalities in the ventricular repolarization phase.

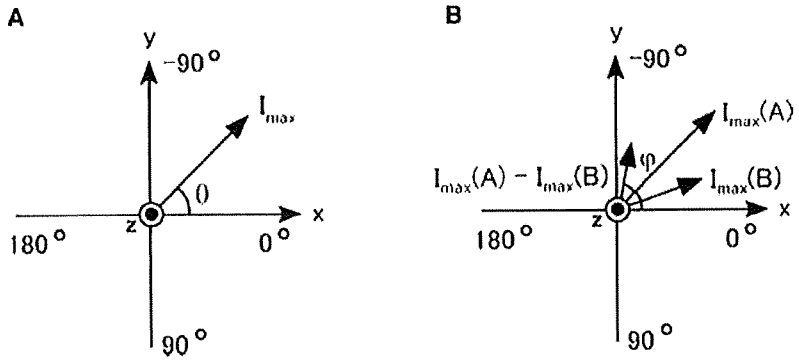

Figure 3. *Definition of current angle (range: +0 to +180 degrees and −0 to −180 degrees). (A) Definition of angle of maximal current vector (MCV). I_{max} indicates maximal current vectors. (B) Definition of angle of difference current vector. I_{max} (A) and I_{max} (B) indicate maximal current vectors at time instants A and B, respectively. I_{max} (A) − I_{max} (B) show the difference current vector.*

Total Current Vector

The TCV based on the CAM is reflected simply to the electrical axis of the heart.[15,16] TCV (I_{TCV} = (I_x, I_y)) is calculated as a vector value by using current vector ($\mathbf{I}_n$) at each sensor,

$$\mathbf{I}_{TCV} = \sum_{n=1}^{64} \mathbf{I}_n(T), \qquad (6)$$

where T indicates the calculated time. We calculated the "amplitude ratio (I_{TCV})," "angle (θ_{TCV})," and "angle of difference current vector (φ_{TCV})" of TCV at four time instants (T_1, T_2, T_p, and T_e) as a spatial-time current parameter. Then, TCV parameters (I_{TCV}, θ_{TCV}, and φ_{TCV}) are calculated in order to substitute TCV vectors (I_x, I_y, and I_{TCV}) for current vectors ($I_{x,max}$, $I_{y,max}$, and I_{max}) in Equations (3)–(5). The definitions of θ_{TCV} and φ_{TCV} are the same as that for the MCV angle (Fig. 2).

Current Integral Map

The CIM is a method of heart disease analysis based on CAM.[17–19] This map represents the amount of current during ventricular depolarization and repolarization. CIM is obtained through the summation of amplitude of current arrows (I_n) during ventricular depolarization and repolarization phases. CIM consists of two parameters ($JTi/QRSi_{max}$ and $JTi/QRSi_{sum}$). The $JTi/QRSi_{max}$ parameter is the ratio of the maximum integral values during ventricular depolarization and repolarization phases, and $JTi/QRSi_{sum}$ is the ratio of the summed current integral values for all channels during ventricular depolarization and repolarization phases.

Current Rotation

CR represents the degree of rotation of the 2D current vector.[21] This value can quantify change in a current distribution pattern. The CR value (I_{rot}) at the n^{th} measurement point is calculated from the following equation (see Fig. 4)

$$Irot_n = \frac{I_{y,n+1} - I_{x,n-8} - I_{y,n-1} + I_{x,n+8}}{I_{n,max}}, \qquad (7)$$

where $I_{n,max}$ denotes the maximal amplitude of CAM for all sensors. CR parameters consist of maximal ($Irot_{max}$) and minimal ($Irot_{min}$) values of $Irot_n$ at time instant T_p, and the difference value (dIrot) between maximal ($Irot_{max}$) and minimal ($Irot_{min}$) values of $Irot_n$.

Statistical Analysis of MCG Parameters

To verify whether it was possible to discriminate between patients with CHD from normal controls using the 25 MCG parameters (MCV, TCV,

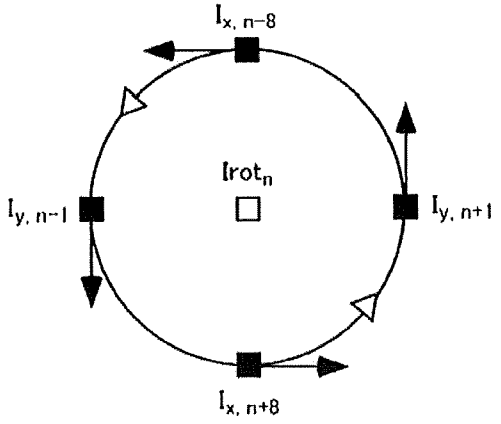

Figure 4. *Rotation direction for summation ($Irot_n$ = $I_{y,n+1} - I_{x,n-8} - I_{y,n-1} + I_{x,n+8}$).*

CIR, and CR), we calculated the area under the receiver operating characteristic (ROC) curve (A_z value).[25] The ROC curve is an index of diagnostic accuracy, and a ROC graph is a plot of all of the sensitivity/specificity pairs resulting from continuously varying the decision threshold for MCG parameters. Here, we use four MCG parameters with a high A_z value ($A_z \geq 0.75$) to detect patients with CHD.

Detection Criterion for CHD Using MCG Parameters

In the MCG test to detect CHD patients, normal ranges of four MCG parameters were determined by an optimal decision threshold that gave the maximum value of the sum of sensitivity and specificity. Furthermore, each MCG parameter was assigned a score of "0" or "1" based on the normal range for an individual subject. Then, the total score of four MCG parameters was calculated. This total score was in the range from "0" to "4." Based on the assumption that a subject with a total score over "1" was strongly suspected of having CHD, we were able to distinguish electrical current abnormalities in CHD patients. We call this total score the repolarization abnormal score. To evaluate the effectiveness of this criterion, the sensitivity and specificity of the MCG test were calculated.

Results

Evaluation of MCG Parameters Based on Current Distributions

Table II lists the A_z values of all MCG parameters. MCG parameters with a high A_z value ($A_z \geq 0.75$) are marked with an asterisk (*). As indicated in the table, seven MCG parameters had a high A_z value.

Maximum Current Vector

MCV angles had high A_z values. In particular, the MCV angle at the T-wave peak (θ_{MCV} (T_p)) had the maximum A_z value (0.808) of all MCV parameters. The angle of difference current vector (φ_{MCV} (T_p, T_2) and φ_{MCV} (T_p, T_e)) also had high A_z values (0.755 and 0.780). On the contrary, the A_z values of MCV amplitude were low (0.572–0.704).

Total Current Vector

The A_z value of the TCV angle at the T-wave peak (θ_{TCV} (T_p)) was 0.832, the maximum A_z value of all MCG parameters. Furthermore, the angle of difference current vector (φ_{TCV} (T_p, T_2) and φ_{TCV} (T_p, T_e)) also had high A_z values (0.801 and 0.792). These A_z values of TCV angle and angular difference were notably higher than those of MCV. However, as in the case of MCV, the A_z values of the amplitude during the ventricular depolarization phase were low (0.534–0.697).

Table II.

MCG Parameters and Their A_z Values. The 25 MCG Parameters Are Categorized as MCV, TCV, CIM, and CR

Parameter Group	Name	Unit	A_z
MCV			
Amplitude	I_{MCV} (T_2, T_1)	–	0.572
	I_{MCV} (T_p, T_2)	–	0.704
	I_{MCV} (T_p, T_e)	–	0.594
Angle	θ_{MCV} (T_1)	degree	0.613
	θ_{MCV} (T_2)	degree	0.643
	θ_{MCV} (T_p)	degree	0.808*
	θ_{MCV} (T_e)	degree	0.743
Angle of difference current vector	φ_{MCV} (T_2, T_1)	degree	0.689
	φ_{MCV} (T_p, T_2)	degree	0.755*
	φ_{MCV} (T_p, T_e)	degree	0.780*
TCV			
Amplitude	I_{TCV} (T_2, T_1)	–	0.644
	I_{TCV} (T_p, T_2)	–	0.697
	I_{TCV} (T_p, T_e)	–	0.534
Angle	θ_{TCV} (T_1)	degree	0.689
	θ_{TCV} (T_2)	degree	0.681
	θ_{TCV} (T_p)	degree	0.832*
	θ_{TCV} (T_e)	degree	0.760*
Angle of difference current vector	φ_{TCV} (T_2, T_1)	degree	0.708
	φ_{TCV} (T_p, T_2)	degree	0.801*
	φ_{TCV} (T_p, T_e)	degree	0.792*
CIM	$JTi_{max}/QRSi_{max}$	–	0.641
	$JTi_{sum}/QRSi_{sum}$	–	0.646
CR	$Irot_{max}$	–	0.607
	$Irot_{min}$	–	0.673
	dI_{rot}	–	0.661

*$A_z > 0.75$

A_z = area under the ROC curve; ROC curve = receiver operating characteristic curve; MCV = maximal current vector; TCV = total current vector; CIM = current integral map; CR = current rotation

Current Integral Map and Current Rotation

The A_z values of maximum and summation integral values ($JTi_{max}/QRSi_{max}$ and $JTi_{sum}/QRSi_{sum}$) were higher than 0.60, and there was not much difference between $JTi_{max}/QRSi_{max}$ and $JTi_{sum}/QRSi_{sum}$. In contrast, CR parameters ($Irot_{max}$ (T_p), $Irot_{min}$ (T_p), and dIrot (T_p)), had low A_z values (0.607–0.673).

These results indicate that current angles (MCV and TCV angles) at the T-wave peak were most effective for distinguishing electrical current abnormalities in CHD patients. Furthermore, angle of difference current vector (MCV and TCV) during the ST-T segment also had high detection accuracy for patients with CHD.

Table III.

Normal Ranges of Four MCG parameters (θ_{MCV} (T_p), θ_{TCV} (T_p), θ_{TCV} (T_p-T_2), and θ_{TCV} (T_p-T_e))

Parameter Name	Unit	Normal Range
θ_{MCV} (T_p)	degree	$6^\circ < \theta_{MCV}$ (T_p) $< 88^\circ$
θ_{TCV} (T_p)	degree	$16^\circ < \theta_{TCV}$ (T_p) $< 69^\circ$
φ_{TCV} ($T_p > T_2$)	degree	$27^\circ < \varphi_{TCV}$ (T_p, T_2) $< 59^\circ$
φ_{TCV} ($T_p > T_e$)	degree	$2^\circ < \varphi_{TCV}$ (T_p, T_e) $< 82^\circ$

Detection of Electrical Current Abnormalities in CHD Patients Using MCG Parameters

Criteria

To detect the electrical current abnormalities in CHD patients, we used four MCG parameters (θ_{MCV} (T_p), θ_{TCV} (T_p), (φ_{TCV} (T_p, T_2), and (φ_{TCV} (T_p, T_e)) with high A_z values. Table III presents the normal ranges of four MCG parameters, which were determined by an optimal decision threshold. This threshold gave the maximum values of the sum of sensitivity and specificity obtained from the ROC curve (see Fig. 5). The ROC curve of θ_{TCV} (T_p) is plotted in Figure 5.

Scoring

Figure 6 illustrates the percentage distributions of subjects—both normal controls (left) and CHD patients (right)—with each repolarization abnormal score ("0" to "4") of the four MCG parameters. We see from Figure 5 that the percentage of normal subjects with a repolarization abnormal score of "0" was 74.3%. In contrast, the percentage of CHD patients with a repolarization abnormal score of "0" was about 15%. Therefore, based on the assumption that a subject with a repolarization abnormal score over "1" is strongly suspected of having CHD, the sensitivity and specificity of the MCG test were 85.7% and 74.3%, respectively.

Figure 7 shows the averaged repolarization abnormal score for normal controls and for patients with SVD, DVD, and TVD. The averaged repolarization abnormal score for normal controls was the lowest ("0.53"). On the other hand, the averaged repolarization abnormal score for patients with TVD was "2.67." This score was high compared to the averaged repolarization abnormal score for patients with SVD and DVD.

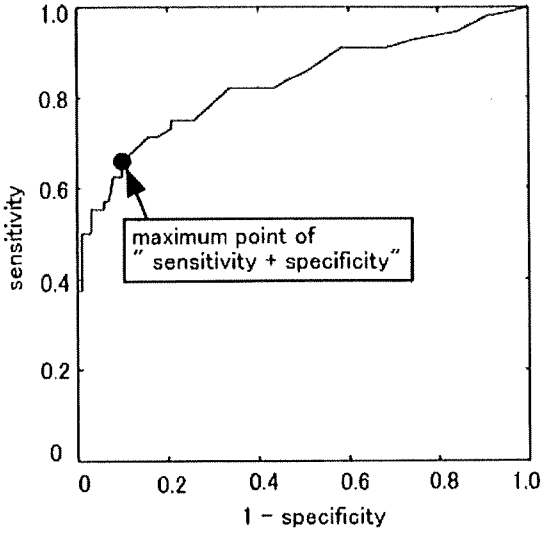

Figure 5. *Receiver operating characteristic curve of total current vector (TCV) angle (θ_{TCV} (T_p)). The black circle shows the maximum point of the sum of sensitivity and specificity.*

Discussion

High Accuracy for Detection of CHD Using MCV and TCV

MCV and TCV angles during the ST-T segment had high A_z values. In myocardial ischemia and infarction, the action potential at the site of a lesion changes significantly. For example, it may disappear or exhibit prolonged ventricular repolarization and prolonged discharge intervals.[26,27] These abnormal action potentials in the ischemic myocardium change the direction of cardiac electrical current. Therefore, it is highly possible that MCV and TCV angles could be used to detect spatial current abnormalities in myocardial ischemia and infarction.

However, angle of difference current vector (MCV and TCV) during ventricular repolarization also resulted in high detection accuracy for CHD patients. In ECG studies, abnormal T waves (tall, flattened, inverted, and biphasic) are caused by myocardial ischemia and infarction influences.[28] These abnormal T waves indicate that the direction of electrical current in the ischemic myocardium changes temporally. Therefore, it is conceivable that the angle of difference current vector reflect time-sequential changes due to current direction dispersion in ischemic myocardium.

In the statistical analysis of CDPs (see Table II), each A_z value of TCV angle and angle of difference current vector were notably higher than that of MCV. In a previous study, the TCV angle during the ventricular repolarization phase was stable with low standard deviation in the case of all age groups that were evaluated.[22] Furthermore, it is noted that with TCV it is possible to detect very low electrical current in a fetal heart.[16] It can, therefore, be concluded that TCV is a useful

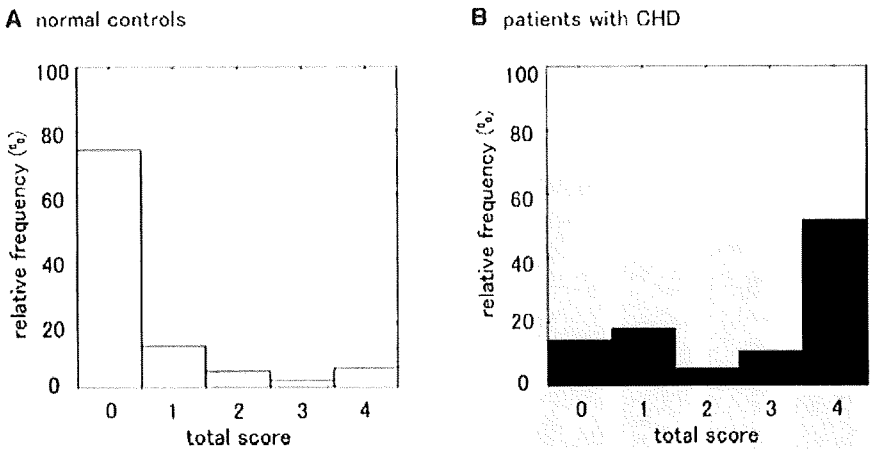

Figure 6. *Percentage distributions of the number of subjects with each repolarization abnormal score (white bars: normal controls, black bars: coronary heart disease patients).*

parameter that is less affected by individual variables such as age and amplitude of cardiac current.

As can be seen, TCV angle and angle of difference current vector difference could accurately detect patients with coronary heart lesions with a vessel diameter over 75%. Therefore, it might be able to detect coronary stenoses of less than 50% diameter, which are clinically significant, in the same way.

Comparison between CDPs and MFPs

Some clinical studies based on MFPs for detection of CHD have been done. Table IV lists the sensitivities and specificities of three MCG tests using MFPs and CDPs.

Park et al. examined four MFPs (method I) taken from the MCG signals during the ventricular repolarization phase for 185 patients with ischemic syndrome.[12] In their study, sensitivity and specificity for the patients were 86.4% and 82.5% using automatic diagnosis. We applied method I for our data listed in Table I. Consequently, sensitivity had a similar value (85.7%), but specificity had a lower value (64.4%). Tolstrup et al. investigated seven MFPs (method II) during ventricular repolarization obtained from 125 patients experiencing chest pain.[13] The sensitivity and specificity of seven MFPs were 76.4% and 74.3%. Hailer et al. examined the semiautomated classification system (method III), which is based on the dipolar structure of current density vector (CDV) map and the direction of the main CDVs, for patients with coronary artery disease patients.[29,30] The calculation of 2D CDV map is based on the inverse problem solution. Sensitivity and specificity for the patients were 73.3% and 70.1%. On the other hand, sensitivity and specificity of the MCG test done using our CDPs were 85.7% and 74.3%. Although each study used different criteria and subjects, these results indicate that the CDPs and MFPs had a similar sensitivity and specificity range from 70% to 85%.

Using the normal ranges of four CDPs established from normal MCG, we obtained a high sensitivity (85.7%) in the CHD patients. Furthermore, the average repolarization abnormal score of four CDPs in the CHD group with severe TVD was higher (2.67) than in the other groups (normal control: 0.53). There is a strong possibility that the repolarization abnormal score correlated with the number of major stenotic vessels. This result indicates the scoring method using four CDPs reflected the electrical activation dispersion due to ischemia and ischemic (infarct) area. It was concluded that CDPs may help to diagnose spatial-time current abnormalities in the myocardium during ventricular repolarization.

Table IV.

Sensitivity and Specificity of MCG Test for Detection of CHD

	Sensitivity	Specificity
Current distribution parameters (CDPs)		
Our result	85.7%	74.3%
Method III[30]	73.3%	70.1%
Magnetic field parameters (MFPs)		
Method I[12]	86.4% (85.7%*)	82.5% (64.4%*)
Method II[13]	76.4%	74.3%

*Sensitivity and specificity of Method I were applied for our data listed in Table I.

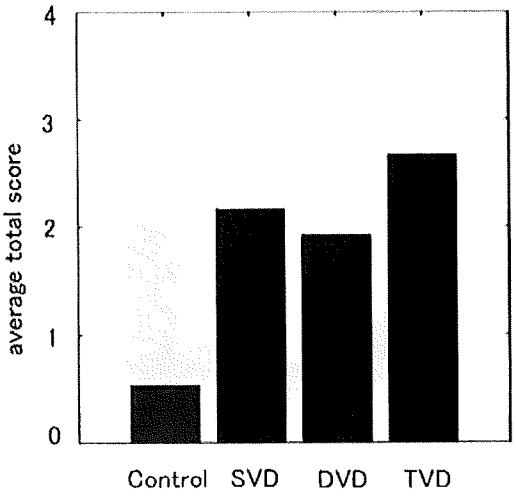

Figure 7. *Averaged repolarization abnormal score of normal controls and patients with single-vessel disease, double-vessel disease, and triple-vessel disease TVD.*

To verify that the CDPs reflect ischemic and infarction size, we calculated the correlations between four CDPs (θ_{MCV} (T_p), θ_{TCV} (T_p), φ_{TCV} (T_p, T_2), and φ_{TCV} (T_p, T_e)) and left ventricular ejection fraction (LVEF). LVEF is an important marker of the left ventricular dysfunction and reflects ischemic and infarct size. Figure 8A–D shows the scatter plots of LVEFs against the four CDPs (θ_{MCV} (T_p), θ_{TCV} (T_p), φ_{TCV} (T_p, T_2), and φ_{TCV} (T_p, T_e)) for 16 patients with CHD. Here, we normalized each CDP by using their median value for healthy volunteers. Figure 8A–D also shows the fitted regression lines calculated for the scatter plots. Average LVEF was 55 ± 14% and ranged from 34% to 75% in the 16 patients. The correlation coefficients between the LVEF and four CDPs were less than −0.35. In particular, φ_{TCV} (T_p, T_e) had the highest correlation ($r = -0.59$). This result might indicate that the level of repolarization current abnormality is associated with ischemic left ventricular dysfunction due to ischemia.

Study Limitations

We should point out several limitations in this study. First, the control group was identified from only the ECG results. Therefore, cardiac hypertrophy, dilation, and HBP, which are detected by other heart functional tests, cannot be excluded in this study. Second, it is not enough to compare the results gotten from the MCG parameters with other heart function parameters (BP, ejection fraction, and ST elevation). In particular, we need to investigate whether abnormal CDPs in

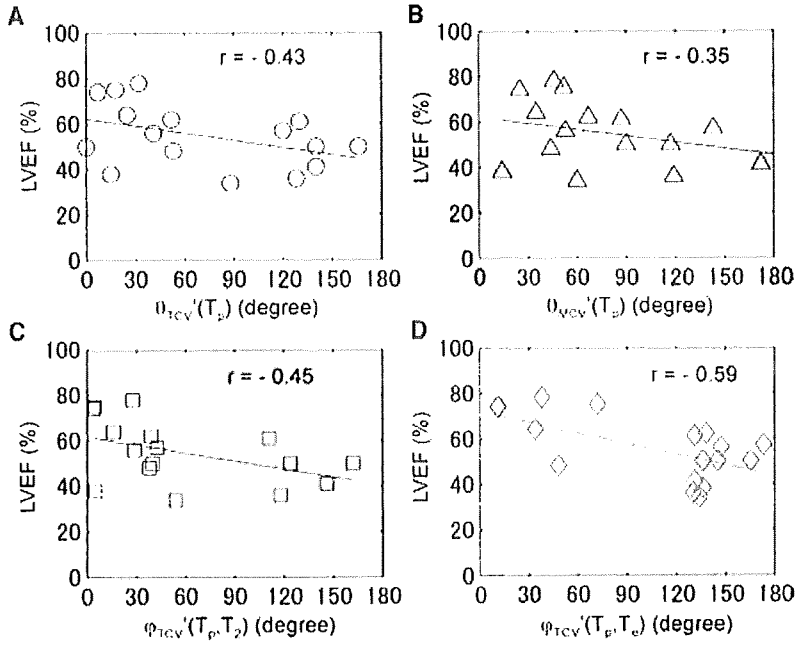

Figure 8. *Scatter plots of left ventricular ejection fractions against the four current distribution parameters (CDPs). (A) θ_{MCV} (T_p), (B) θ_{TCV} (T_p), (C) φ_{TCV} (T_p, T_2), and (D) φ_{TCV} (T_p, T_e)). We normalized each CDP by using their median value for healthy volunteers.*

CHD patients result from CHD or high BP, since half of CHD patients generally had HBP. Third, we defined the coronary heart lesions as a vessel diameter over 75%. Fourth, the number of patients with CHD (56 patients) was small.

Despite these limitations, the repolarization abnormal score and criteria using four CDPs in CHD patients can reflect lesion size and time changes of electrical activation dispersion due to ischemia.

Future Work

To evaluate the improvement in cardiac function, we will compare the CDPs of CHD patients before and after coronary revascularization. We also consider it important to distinguish abnormalities in ventricular repolarization for CHD patients with diabetes, hypertension, hypertrophy, and rhythm conductance abnormalities by using CDP.

Acknowledgments: We gratefully thank Noriko Takuma, Nobuo Sasaki of Hitachi General Hospital, Satsuki Yamada of Mayo Clinic, and Keiji Tsukada of Okayama University for their valuable advice. Furthermore, we are also grateful to Shigeaki Naito, Toru Okihara, Hiroki Ihara, Hiroyuki Suzuki, and Masahiro Murakami of Hitachi-High Technologies Corporation for planning the MCG measurements.

References

1. Mackay J, Mensah G. Atlas of heart disease and stroke. Geneva: World Health Organization, 2004.
2. Ikeda K, Kamimura H. Studies on characteristics of cause of death in Japan. Tokyo Metropolitan Research Laboratory of Public Health Annual Reports 1998; 41:1–4.
3. Fortuin NJ, Weiss JL. Exercise stress testing. Circulation 1977; 56:699–712.
4. Polizos G, Ghamsary M, Ellestad MH. The severity of myocardial ischemia can be predicted by the exercise electrocardiogram. Cardiology 2005; 104:215–220.
5. Gianrossi R, Detrano R, Mulvihill D, Lehmann K, Dubach P, Colombo A, McArthur D, et al. Exercise-induced ST depression in the diagnosis of coronary artery disease. A meta-data. Circulation 1989; 80:87–98.
6. Cohen D, Lepeschkin E, Hosaka H, Massell BF, Myers G. Abnormal patterns and physiological variations in magnetocardiograms. J Electrocardiol 1976; 9:398–409.
7. Hoeing HE, Daalmans GM, Bar L, Bommel F, Paulus A, Uhl D, Weisse HJ, et al. Multi channel DC SQUID sensor array for biomagnetic applications. IEEE Trans Magn 1991; 27:2777–2785.
8. Drung D, Koch H. An electrical second-order gradiometer for biomagnetic applications in clinical shielded rooms. IEEE Trans Appl Supercond 1993; 3:2594–2597.
9. Tsukada K, Haruta Y, Adachi A, Ogata H, Komuro T, Ito T, Takada Y, et al. Multichannel SQUID system detecting tangential components of the cardiac magnetic field. Rev Sci Instrum 1995; 66:5085–5091.
10. Tsukada K, Kandori A, Miyashita T, Sasabuchi H, Suzuki H, Kondo S, Komiyama Y, et al. A simplified superconducting quantum interference device system to analyze vector components of a cardiac magnetic field. Proc 20th Int Conf IEEE/EMBS 1998; 524–527.
11. Seki Y, Kandori A, Suzuki D, Ohnuma M. Open-type magnetocardiograph with cylindrical magnetic shield. Appl Phys Lett 2005; 86:243902.
12. Park JW, Jung F. Qualitative and quantitative description of myocardial ischemia by means of magnetocardiography. Biomed Technik 2004; 49:267–273.
13. Tolstrup K, Madsen BE, Ruiz JA, Greenwood SD, Camacho J, Siegel RJ, Gertzen HC. Non-invasive resting magnetocardiographic imaging for the rapid detection of ischemia in subjects presenting with chest pain. Cardiology 2006; 106:270–276.
14. Miyashita T, Kandori A, Tsukada K, Sato M, Terada Y, Horigome H, Mitsui. Construction of tangential vectors from normal cardiac magnetic field components. Proc 20th Int Conf IEEE/EMBS 1998; 520–523.
15. Kandori A, Kanzaki H, Miyatake K, Hashimoto S, Ito S, Tanaka N, Miyashita, et al. A method for detecting myocardial abnormality by using a total current-vector calculated from ST-segment deviation of a magnetocardiogram signal. Med Biol Eng Comput 2001; 39: 21–28.
16. Kandori A, Miyashita T, Tsukada K, Hosono T, Miyashita S, Chiba Y, Horigome H, et al. Prenatal diagnosis of QT prolongation by fetal magnetocardiogram-use of QRS and T-wave current-arrow maps. Physiol Meas 2001; 22:377–387.
17. Tsukada K, Miyashita T, Kandori A, Mitsui T, Terada Y, Sato M, Shiono J, et al. An iso-integral technique using magnetocardiogram, and its possible use for diagnosis of ischemic heart disease. Int J Cardiac Imaging 2000; 16:55–66.
18. Shiono J, Horigome H, Matsui A, Terada Y, Watanabe S, Miyashita T, Tsukada K. Evaluation of myocardial ischemia in Kawasaki disease using an isointegral map on magnetocardiogram. Pacing Clin Electrophysiol 2002; 25:915–921.
19. Yamada S, Yamaguchi I. Magnetocardiograms in clinical medicine: Unique information on cardiac ischemia, arrhythmias, and fetal diagnosis. Intern Med 2005; 44:1–19.
20. Kandori A, Kanzaki H, Miyatake K, Hashimoto S, Ito S, Tanaka N, Miyashita T, et al. A method for detecting myocardial abnormality by using a current-ratio map calculated from an exercise-induced magnetocardiogram. Med Biol Eng Comput 2001; 39: 29–34.
21. Kanzaki H, Nakatani S, Kandori A, Tsukada K, Miyatake K. A new screening method to diagnose coronary artery disease using multichannel magnetocardiogram and simple exercise. Basic Res Cardiol 2003; 98:124–132.
22. Kandori A, Ogata K, Watanabe Y, Takuma N, Tanaka K, Murakami M, Miyashita T, et al. Space-time database for standardization of adult magnetocardiogram—making basic MCG standard parameters. Pacing Clin Electrophysiol (to be published).
23. Kandori A, Oe H, Miyashita K, Miyashita T, Ohira S, Naritomi H, Chiba Y, et al. Magneto-encephalographic measurement of neural activity during period of vertigo induced by cold caloric stimulation. Neuerosci Res 2003; 46: 281–288.
24. Miyashita T, Kandori A, Tsukada K, Yamada S, Shiono J, Horigome H, Terada Y, et al. Multiple-current-vector diagrams for evaluating inhomogeneity of myocardial activity – applied to ischemic heart disease and cardiomyopathy. Proc 13th Int Conf BIOMAG 2002; 582–583.
25. Zweig MH, Campbell G. Receiver-operating characteristic (ROC) plots: A fundamental evaluation tool in clinical medicine. Clin Chem 1993; 39:561–577.
26. Cinca J, Janse MJ, Morena H, Candell J, Valle V, Durrer D. Mechanism and time course of the early electrical changes during acute coronary artery occlusion. An attempt to correlate the early ECG changes in man to the cellular electrophysiology in the pig. Chest 1980; 77:499–505.
27. Downar R, Janse MJ, Durrer D. The effect of acute coronary occlusion on subepicardial transmembrane potentials in the intact porcine heart. Circulation 1977; 56:217–224.
28. Channer K, Morris F. ABC of clinical electrocardiography: Myocardial ischemia. BMJ 2002; 324:1023–1026.
29. Hailer B, Chaikovsky I, Auth-Eisernitz S, Schäfer H, Steinberg F, Grönemeyer DH. Magnetocardiography in coronary artery disease with a new system in an unshielded setting. Clin Cardiol 2003; 26:465–471.
30. Hailer B, Chaikovsky I, Auth-Eisernitz S, van Leeuwen P. The value of magnetocardiography in patients with and without relevant stenoses of the coronary arteries using an unshielded system. Pacing Clin Electrophysiol 2005; 28:8–16.

RESEARCH ARTICLE

Human Mutation

OFFICIAL JOURNAL
HGVS
HUMAN GENOME VARIATION SOCIETY
www.hgvs.org

Novel KCNE3 Mutation Reduces Repolarizing Potassium Current and Associated With Long QT Syndrome

Seiko Ohno,[1] Futoshi Toyoda,[2] Dimitar P Zankov,[2,3] Hidetada Yoshida,[1] Takeru Makiyama,[1] Keiko Tsuji,[3] Toshihiro Honda,[4] Kazuhiko Obayashi,[5] Hisao Ueyama,[6] Wataru Shimizu,[7] Yoshihiro Miyamoto,[8] Shiro Kamakura,[7] Hiroshi Matsuura,[2] Toru Kita,[1] and Minoru Horie[3]*

[1]*Department of Cardiovascular Medicine, Kyoto University Graduate School of Medicine, Kyoto, Japan*

[2]*Department of Physiology, Shiga University of Medical Science, Shiga, Japan*

[3]*Department of Cardiovascular and Respiratory Medicine, Shiga University of Medical Science, Shiga, Japan*

[4]*Cardiovascular Center, Saiseikai Kumamoto Hospital, Kumamoto, Japan*

[5]*Obayashi Clinic, Kyoto, Japan*

[6]*Department of Molecular Medical Biochemistry, Shiga University of Medical Science, Shiga, Japan*

[7]*Division of Cardiology, Department of Internal Medicine, National Cardiovascular Center, Osaka, Japan*

[8]*Laboratory of Molecular Genetics, National Cardiovascular Center, Osaka, Japan*

Communicated by Claude Férec

Received 25 January 2008; accepted revised manuscript 5 May 2008.
Published online 20 March 2009 in Wiley InterScience (www.interscience.wiley.com). DOI 10.1002/humu.20834

ABSTRACT: Long QT syndrome (LQTS) is an inherited disease involving mutations in the genes encoding a number of cardiac ion channels and a membrane adaptor protein. Among the genes that are responsible for LQTS, *KCNE1* and *KCNE2* are members of the *KCNE* family of genes, and function as ancillary subunits of Kv channels. The third *KCNE* gene, *KCNE3*, is expressed in cardiac myocytes and interacts with *KCNQ1* to change the channel properties. However, *KCNE3* has never been linked to LQTS. To investigate the association between *KCNE3* and LQTS, we conducted a genetic screening of *KCNE3* mutations and single nucleotide polymorphisms (SNPs) in 485 Japanese LQTS probands using DHPLC-WAVE system and direct sequencing. Consequently, we identified two *KCNE3* missense mutations, located in the N- and C-terminal domains. The functional effects of these mutations were examined by heterologous expression systems using CHO cells stably expressing KCNQ1. One mutation, p.R99λH was identified in a 76-year-old woman who suffered torsades de pointes (TdP) after administration of disopyramide. Another mutation, p.T4A was identified in a 16-year-old boy and 67-year-old woman. Although the boy carried another *KCNH2* mutation, he was asymptomatic. On the other hand, the woman suffered from hypokalemia-induced TdP. In a series of electrophysiological analyses, the KCNQ1(Q1)+KCNE3(E3)-R99λH channel significantly reduced outward current compared to Q1+E3-WT, though the current density of the Q1+E3-T4A channel displayed no statistical significance. This is the first report of *KCNE3* mutations associated with LQTS. Screening for variants in the *KCNE3* gene is of clinical importance for LQTS patients.
Hum Mutat 30, 557–563, 2009. © 2009 Wiley-Liss, Inc.

KEY WORDS: long QT syndrome; LQTS; *KCNE3*; ion channel; molecular screening; electrophysiology

Introduction

Long QT syndrome (LQTS) is an inherited disease characterized by a prolonged QT interval and a high risk of sudden cardiac death due to peculiar ventricular tachycardia known as torsades de pointes (TdP) [Moss and Kass, 2005]. Most of the LQTS-causing genes encode ion channels, with particular regard to potassium (K) channels. Among them, *KCNE1* (E1) and *KCNE2* (E2) are members of the *KCNE* family (E1 through *KCNE5*) encoding a single-transmembrane-domain proteins. They are called MinK-related peptides (MiRPs) that function as ancillary subunits of Kv channels. In 1999, the third *KCNE* gene, *KCNE3* (ONIM *604433) (E3), was cloned by homology to E1 [Abbott et al., 1999]. In the functional analysis on the KCNQ1 (Q1) +E3 channel, E3 was shown to markedly change Q1 channel properties to yield those activating nearly instantaneously and linearly on voltage [Schroeder et al., 2000].

The expression of E3 in heart was examined and confirmed by northern blot analysis [Schroeder et al., 2000], real-time quantitative RT-PCR [Bendahhou et al., 2005; Lundquist et al., 2005, 2006] and in situ hybridization [Lundquist et al., 2005]. E3 was expressed in all regions of the human heart including left and right ventricles [Lundquist et al., 2005]. The expression level of E3 was larger than that of E2 in every region of the human heart, although smaller than that of E1 [Bendahhou et al., 2005; Lundquist et al., 2005, 2006]. Recently, E3 was reported to

S.O. and F.T. contributed equally to this work.

*Correspondence to: Minoru Horie, M.D., Ph.D., Department of Cardiovascular and Respiratory Medicine, Shiga University of Medical Science, Seta Tsukinowa-cho, Otsu, Shiga, Japan 520-2192. E-mail: horie@belle.shiga-med.ac.jp

Contract grant sponsor: Japan Society for the Promotion of Science; Contract grant sponsor: Ministry of Health, Labour and Welfare, Japan; Grant number: H18-Research on Human Genome-002.

establish a complex with Q1 along with E1 [Morin and Kobertz, 2007]. The Q1+E1+E3 complex generated the current with the combined properties of homomeric Q1+E1 and Q1+E3 complexes, as we previously reported the properties of Q1+E1+E2 complexes [Toyoda et al., 2006]. Taken together, the dysfunction of the Q1+E3 channel may reduce repolarizing K currents in the myocardium, which thereby prolongs the QT interval, although Q1–E3 channels have not yet been demonstrated in the heart.

Abbott et al. [2001] demonstrated a missense mutation of E3 (p.R83λH) in the patients of periodic paralysis. The reduced current densities of the E3-R83λH plus Kv3.4 complex channel in the skeletal muscle caused periodic paralysis, though the authors did not mention cardiac symptoms. More recently, Lundby et al. [2008] identified an E3 mutation (p.V17λM) from an early-onset lone atrial fibrillation (AF) patients. They performed functional analysis of E3-V17λM in coexpression with five kinds of potassium channels. As a result, they revealed increased activity of KV4.3+E3-V17λM and KCNH2+E3-V17λM channels.

During the genetic screening on 485 Japanese LQTS probands, we identified two novel E3 mutations and one reported single nucleotide polymorphism (SNP) (rs34604640:C>G; p.P39R). The mutations were p.T4A in the N-terminal and p.R99λH in the C-terminal. In the present study, we describe the clinical phenotypes of E3-related LQTS patients and the electrophysiological effects caused by these E3 mutations, and assess the probability of E3 as a candidate gene for LQTS.

Materials and Methods

Subjects

Study patients are comprised of 485 congenital and acquired LQTS probands showing prolongation of the QT interval (QTc≥460 ms) or documented TdP from 485 unrelated families. They were referred consecutively to either of our laboratories for genetic evaluation. All subjects submitted written informed consent in accordance with the guidelines approved by each institutional review board. Each underwent detailed clinical and cardiovascular examinations, and were then characterized on the basis of the QT interval in lead V_5 corrected for heart rate (QTc) according to Bazett's formula and the presence of cardiac symptoms.

Genotyping

Genomic DNA was isolated from venous blood lymphocytes as previously described [Ohno et al., 2007]. Through PCR, denaturing high-performance liquid chromatography (DHPLC), and direct DNA sequencing, we performed a comprehensive open reading frame/splice-site mutational analysis of known LQTS genes (*KCNQ1*, *KCNH2*, *SCN5A*, *KCNE1*, and *KCNE2*) using previously described primers [Ohno et al., 2007]. We did not conduct mutational analysis of *ANKB*, *KCNJ2*, *CACNA1C*, *CAV3*, and *SCN4B*. The *KCNE3* coding region was amplified with a primer pair; forward primer; 5′-CTGAGCTTCTACCGAGTCTT-3′ and reverse primer; 5′-TGCAGTCCACAGCAGAGTTC-3′. The size of the PCR product was 435 base pairs. DHPLC analysis of *KCNE3* was performed at three different temperatures; 59.0, 61.2, and 63.5°C. The cDNA sequence was based on GenBank reference sequence NM_005472.4, and the numbering reflects cDNA numbering with +1 corresponding to the A of the ATG translation initiation codon in the reference sequence, according to journal guidelines. The initiation codon is codon 1.

Plasmid Construction

cDNA for human *KCNE3* (NM_005472.4) was cloned into a PCR3.1 plasmid. Variant amino acid residues were constructed using a Quick Change® II XL Site-Directed Mutagenesis Kit (Stratagene, La Jolla, CA), according to the manufacturer's instructions. Nucleotide sequence analysis was performed on each variant construct prior to the expression study.

Construction of a CHO Cell Line Stably Expressing Human KCNQ1

Flp-In CHO cells containing a single integrated Flp recombinase target (FRT) site at a transcriptionally active locus (Invitrogen, Carlsbad, CA) were used for the generation of a stable KCNQ1 cell line. The full-length cDNA fragment of human *KCNQ1* (GenBank AF000571.1) in a pCI vector (a kind gift from Dr. J. Barhanin, Institut de Pharmacologie Moléculaire et Cellulaire, CNRS, Valbonne, France) was subcloned into a pcDNA5/FRT vector (Invitrogen). This construct was cotransfected into Flp-In CHO cells with pOG44, a Flp-recombinase expression vector (Invitrogen), resulting in the targeting interaction of the expression vector. Stable cell clones were selected in hygromycin B (500 μg/ml; Invitrogen), and the expression of KCNQ1 was tested by the whole-cell patch-clamp recording method. One cell line exhibited uniform and homogenous expression of KCNQ1 currents and was used for experiments.

Cell Culture and Transient Transfection

The stable KCNQ1-CHO cell line was maintained in Ham's F-12 medium supplemented with 10% fetal calf serum and 500 &mug/ml hygromycin B in a humidified incubator gassed with 5% CO_2 and 95% air at 37°C. Before transfection, cells were seeded onto 35-mm plastic culture dishes with seven to eight glass coverslips (5λmm × 3λmm) and incubated for 24 to 48λhr. Transient transfection was performed using Lipofectamine (Invitrogen). The amounts of each cDNA used for transfection were (mug/dish): 1.0 *KCNE3*, and 0.5 green fluorescent protein (GFP). At 48 to 72λhr after transfection, only GFP-positive cells were selected for the patch-clamp study.

Patch-Clamp Recordings and Data Analysis

Whole-cell membrane currents were recorded with an EPC-8 patch-clamp amplifier (HEKA, Lambrecht, Germany). A coverslip with adherent CHO cells was placed on the glass bottom of a recording chamber (0.5λml in volume) mounted on the stage of Nikon Diaphot inverted microscope (Tokyo, Japan). Patch pipettes were prepared from glass capillary tube (Narishige, Tokyo, Japan) by means of a Sutter P-97 micropipette puller (Novato, CA), and the tips were then fire-polished with a microforge. Pipette resistance ranged from 2 to 4 Mω when filled with internal solution. Current recordings were conducted at 34±1°C. Voltage-clamp protocols and data acquisition were controlled by PatchMaster software (version 2.03, HEKA) via an LIH-1600 AD/DA interface (HEKA). Cell membrane capacitance (Cm) was measured in every cell by fitting a single exponential function to capacitive transients elicited by 20 ms voltage-clamp steps from a holding potential of −80 mV.

External Tyrode solution contained (mM): 140 NaCl, 0.33 NaH_2PO_4, 5.4 KCl, 1.8 $CaCl_2$, 0.5 $MgCl_2$, 5.4 glucose, and 5 HEPES, and pH was adjusted to 7.4 with NaOH. The internal

pipette solution contained (mM): 70 potassium aspartate, 50 KCl, 10 KH_2PO_4, 1 $MgCl_2$, 3 Na_2-ATP, 0.1 Li_2-GTP, 5 EGTA, and 5 HEPES, and pH was adjusted to 7.2 with KOH. Liquid junctional potential between the test solution and the pipette solution was measured to be around −10 mV and was corrected. HMR1556 (a kind gift from Drs. H.J. Lang and J. Pünter, Aventis Pharma Deutschland GmbH) was added from 10 mM stock solution in DMSO to the external solution (final DMSO concentration did not exceed 0.01%).

To obtain the deactivation time constant, the time course of decaying tail current at −50 mV were fitted to a single exponential function:

$$I(t) = A + B\exp(-t/\tau),$$

where I(t) means the tail current amplitude at time t, A and B are constants, and τ is the deactivation time constant.

All data are presented as mean ± standard error of the mean (SEM). Statistical analysis was performed by analysis of variance (ANOVA) followed by Tukey-Kramer post hoc comparison. Statistical significance was set at $P < 0.05$.

Cell Preparation and Confocal Imaging

For the immunofluorescence study, we constructed a hemagglutinin (HA)-tagged *KCNE3* plasmid (wild type [WT] and mutant). An HA epitope (YPYDVPDYA) was introduced into the N-terminus of *KCNE3* cDNA, using an HA-tagged 5′ primer with a KpnI restriction site at the 5′ end and a 3′ primer with BsrGI at the 3′ end. The full-length cDNA fragment of human *KCNQ1* was subcloned into pCI-neo. COS7 cells were transfected with 1.0 &mug of HA-tagged pCR3.1-*KCNE3* (WT or mutant) and 1.0 &mug of pCI-neo-*KCNQ1* plasmid in 35-mm glass-bottom dishes, using Fugene6 (Roche Diagnostics, Basel, Switzerland) according to the manufacturer's instructions. At 48λhr later, the cells were washed twice with phosphate buffered saline (PBS), followed by incubation with a mouse anti-HA primary antibody (1:500) (Covance Research Products, Inc., Berkeley, CA) for 30λminutes at 37°C. The cells were then washed twice with PBS and incubated with an anti-mouse antibody conjugated to the Alexa 488 fluorophore (1:500) (Molecular Probes, Eugene, OR) as a secondary antibody for 30λminutes at 37°C. Finally, cells were washed with and immersed in Opti-Mem, and confocal images were obtained with a Zeiss LSM 510 (Carl Zeiss GmbH, Jena, Germany).

Results

Mutation Analysis

In 485 LQTS probands, we identified two novel missense mutations and one SNP in E3 (Figs. 1 and 2). The first mutation was a single nucleotide alternation (c.296G>A) (Fig. 1A) resulting in an amino acid substitution from an arginine at residue 99 with a histidine (p.R99λH). The second mutation was a single nucleotide change (c.10A>G) (Fig. 2A), causing an amino acid substitution p.T4A, replacing a threonine at residue 4 with an alanine. This T4A missense mutation was identified in two probands. Another proband was found to have a p.P39R polymorphism, which was reported as an SNP (rs34604640: C>G). These three variants were absent in 200 unrelated healthy individuals (400 alleles) from the general Japanese population. They are located in the N-terminus (T4A and P39R) and C-terminus (R99λH), respectively. We further searched for another mutation in LQTS-related genes in these probands carrying E3 mutations (see Materials and Methods). In one of the KCNE3-T4A carriers, we identified a *KCNH2*-p.G572S mutation and in the proband with the P39R polymorphism a *KCNH2*-p.W563G mutation. SNP c.198 T>C (rs2270676), which causes no amino acid substitution (p.F66F), was identified heterozygously in roughly 20% of both LQTS probands and healthy individuals.

Phenotypic Characterization

Patient 1

The novel mutation p.R99λH was found in a 76-year-old female suffering from drug-induced TdP. Her resting 12-lead electrocardiograph (ECG) before administration of disopyramide (Fig. 1B-a) displayed sinus rhythm with normal QTc (438 ms). Because of repeated paroxysmal AF, she was started on 300λmg of disopyramide per day. At 10 days after disopyramide intake, her level of consciousness decreased and ECGs displayed frequent premature ventricular contractions (PVCs) and TdP (Fig. 1B-b). Her heart rate was 66 beats per minute (bpm), and her QTc time was prolonged to 580 ms. Serum K level was within normal range (4.0 mEq/L). Disopyramide was immediately stopped, and temporary pacing was immediately started at 90 bpm. In 3 days, TdP attacks ceased and QTc intervals returned within normal range. She had no family history of sudden cardiac death and LQTS. We did not conduct genetic analyses on the relatives of this patient, due to a lack of consent.

Patient 2

A p.T4A mutation was identified in a 16-year-old boy who had QT prolongation discovered during his school's annual health checkup. He had no history of faintness or syncope and no family history of syncope or sudden death. His resting ECG (Fig. 2B) revealed bradycardia for age (48 bpm) and QT prolongation (QTc = 525 ms). Genetic analysis on other LQTS-related genes revealed a *KCNH2*-G572S missense mutation which had been previously reported [Tester et al., 2005]. His mother and sister also remained asymptomatic but had the same heterozygous set of genetic variants (E3-T4A and *KCNH2*-G572S). Their ECGs also displayed the prolongation of QTc intervals: 520 ms and 560 ms (data not shown).

Patient 3

A p.T4A mutation was also identified in another unrelated proband, a 68-year-old female, who experienced hypokalemia-induced TdP at age 60 years. After correction of serum potassium levels, her QTc time was normalized to 430 msec (Fig. 2C). Two years after the TdP event, she was diagnosed with cardiac sarcoidosis and was started on steroid hormone therapy. Though her daughter also carried the E3-T4A mutation, she was asymptomatic with borderline QTc.

Patient 4

A p.P39R amino acid substitution was identified in a 32-year-old female who was also identified to have a novel *KCNH2* missense mutation, p.W563G. She experienced repeated episodes of late night syncope at ages 15, 21, and 26 years. Figure 3 displays her 12-lead ECG demonstrating marked QT prolongation (QTc = 512 msec) and notched T waves, suggesting LQTS type

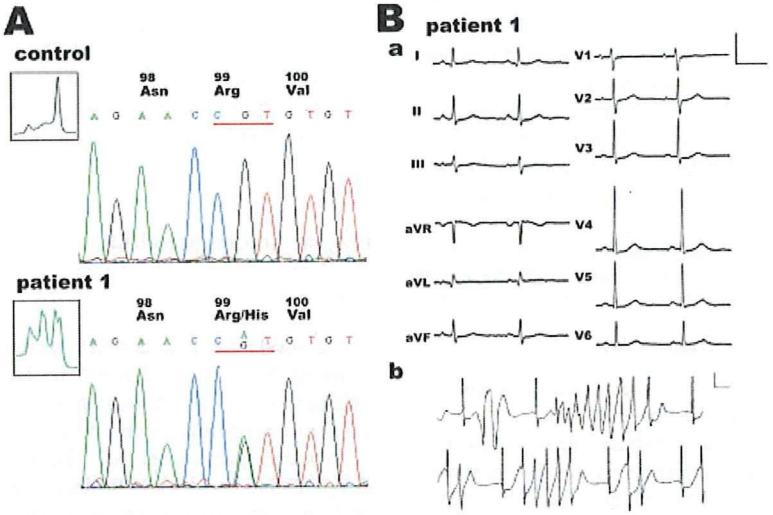

Figure 1. Molecular discovery and clinical characterization of R99H-KCNE3. **A:** DHPLC (insets) and DNA sequence analyses of normal control and Patient 1. DNA sequencing chromatograms demonstrate an arginine (Arg) to histidine (His) substitution at residue 99. **B:** ECGs of Patient 1. (a) 12-lead ECG and (b) monitoring ECG of TdP in a 76-year-old female patient. Scale bars indicate 1 mV and 400 ms. [Color figure can be viewed in the online issue, which is available at www.interscience.wiley.com.]

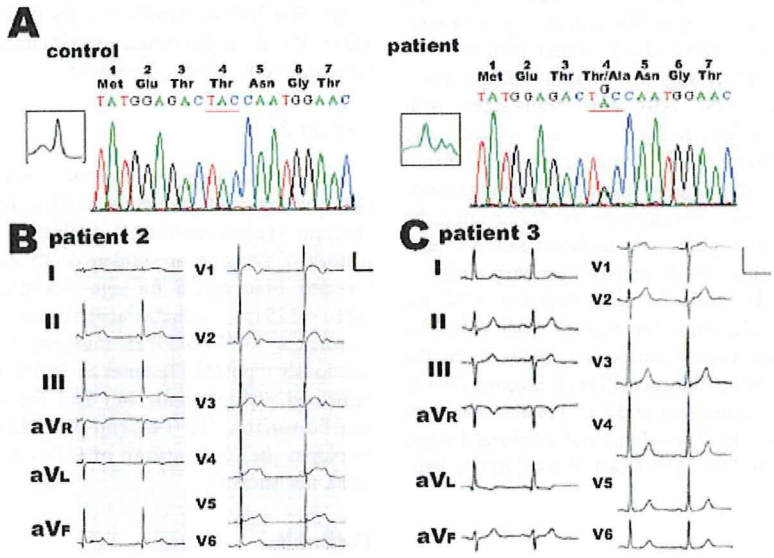

Figure 2. Molecular discovery and clinical characterization of T4A-KCNE3. **A:** DHPLC (insets) and DNA sequence analysis of normal control and patient. DNA sequencing chromatograms demonstrate a threonine (Thr) to alanine (Ala) substitution at residue 4. **B:** The 12-lead ECG of Patient 2. **C:** The 12-lead ECG of Patient 3. [Color figure can be viewed in the online issue, which is available at www.interscience.wiley.com.]

2. E3-P39R was reported as an SNP (rs34604640: C>G); however, P39R was absent in 400 control alleles from healthy Japanese cohorts. Therefore, we conducted a functional analysis of three mutants including P39R.

Biophysical Properties of KCNQ1 Channels Coexpressed With KCNE3

To clarify the functional consequences of these missense mutations (R99λH, T4A, and P39R) on E3, we assessed the biophysical properties of the mutated E3 clone by using the stably expressing human KCNQ1-CHO cell line. Figure 4A shows representative examples of whole-cell currents recorded from CHO cells stably expressing the Q1 channel transfected with or without E3 (WT or mutant). Insets to the right of each recording illustrate expanded views of the tail current elicited after return to –50 mV from test potentials. The current amplitudes were normalized by cell capacitances (current densities). Recordings from cells expressing the Q1 channel alone (left panel of Fig. 4A) displayed small amplitudes of time-dependent outward currents during depolarizing test potentials, followed by slowly deactivating tail currents on return to –50 mV. In contrast, transfection of stable Q1 cells with E3-WT (second panel in Fig. 4A) gave rise to large amplitudes of currents composed of at least two components: 1) a time-dependent outward current activated during depolarizing steps; and 2) a constitutively active background